Mixing Enhancement of Electroosmotic Flow in Microchannels under DC and AC Electric Field

S. Dong†, P. F. Geng, D. Dong and C. X. Li

Department of Power Engineering, North China Electric Power University, Baoding 071003, Hebei, China

†*Corresponding Author Email: shuai.dong@ncepu.edu.cn*

ABSTRACT

A novel micromixer is presented in this study and the effect of DC or AC electric field on mixing efficiency is investigated numerically. Four types of AC waveforms are considered to explore the flow characteristic and mixing efficiency. The velocity field, concentration field and the mixing efficiency are analyzed in details. The results demonstrated that a pair of vortices with opposite rotating directions is generated when DC or AC voltages is applied to the electrode plates planted within the walls. The generated vortices greatly enhance the mixing of incoming fluids with different concentrations. The mixing efficiency firstly rises with time and then reaches a relative stable periodic state under different potential waveforms. As the voltage applied on the plates increases, the mixing efficiency is improved obviously. The mixing efficiency under full-wave AC signal is the highest, and it is up to 95.44% when the applied potential is 3 V and frequency is 5 Hz.

Keywords: Mixing efficiency; Potential waveforms; Numerical simulation; Optimization; Electroosmotic flow; Microchannel.

NOMENCLATURE

C	concentration of fluid	$\mathbf{u}$	velocity vector
c_0	initial concentration at inlet	z	ionic valence
c_m	concentration of fully mixed state		
D_c	diffusion coefficient	ε_0	permittivity of free space
$\mathbf{E}$	electric field strength	ε_r	relative permittivity
e	unit electron charge	μ	dynamic viscosity
f	frequency applied to the electrodes	ζ	zeta potential
k_B	Boltzmann constant	ρ	density
L	height of the outlet	σ	mixing efficiency
n_∞	average concentration of ion	$\overline{\sigma}$	average mixing efficiency in one cycle
p	pressure	φ_{in}	inlet potential
T_0	temperature	ψ	induced electrical potential of the Electrical Double Layers (EDL)
t	time		

1. INTRODUCTION

The lab-on-a-chip (LOC) device is an important technology in the development of micro-total-analysis-system (Nekoubin, 2018; Hamedi *et al.,* 2016). The basic functions of biological or chemical laboratories can be downsized to a few centimeters of chips to simplify the analytical process, reduce consumption of samples and improve the accuracy of analysis (Stone *et al.,* 2004). At present, microfluidic chip has been widely used throughout the food and chemical

industries etc. (Chao *et al.,* 2010a; Auroux *et al.,* 2002; Chen and Cho 2008).

The microfluidic device is usually micron in size, and the flow rate is relatively small, thus the Reynolds number is very small. The flow is essentially laminar and hence efficient turbulent mixing is absent (Ansari *et al.,* 2012; Lee *et al.,* 2016). Therefore, the mixing of two different solutions within a microchannel is achieved only by diffusion mechanisms and it will take a very long time (Lim and Lam, 2012). Many microfluidic devices attempt to overcome this disadvantage by passive method or active method (Shamloo *et al.,* 2017; Matías *et al.,* 2018). The passive mixing method does not require external force (Wang *et al.,* 2007). Usually, a special channel design is implemented to introduce disturbance or vortices in the flow field, such as physical and chemical modification of the solid wall surface, modification of the channel geometry, etc. (Chen *et al.,* 2016).

Chen *et al.* (2017) investigated the mixing characteristic in six different shapes of microchannels. It was found that the microchannel in square-wave shape is the optimal geometry for higher mixing efficiency. Hossain *et al.* (2017) presented a novel design of chaotic micromixer with two-layer serpentine crossing microchannels. High level mixing index has been confirmed in both the numerical and experimental analyses, and mixing efficiency was achieved around 99% at Reynolds numbers less than 10. Alam *et al.* (2014) analyzed the influence of obstacles inside of microchannels on mixing characteristic. It was found that the mixing index of curved microchannels is better than that of T-shaped channels. However, the flow resistance with the obstacles has not been considered carefully. Besides, the microchannels mentioned above have some defects, like high cost, complex designing, fixed characteristics and poor portability (Lee *et al.,* 2011; Rashidi *et al.,* 2018).

In contrast to the passive methods, the active control technology is usually applied to the fluids with some external forces. The mixing is enhanced by changing the direction and speed of the fluids (Xie and Jian, 2017). There are many types of active methods for fluid mixing in microchannels, and the mechanisms can be very different. According to the type of driving force, it can be divided into electroosmotic flow (EOF) (Cheng *et al.,* 2018), electromagnetic driven flow (Kamali *et al.,* 2014), pressure driven flow (Ma *et al.,* 2008), acoustic streaming flow (Yaralioglu *et al.,* 2004) and so on. The flow behavior can be

controlled flexibly by changing the size, direction and placement of the external forces, which results in micro-vortex flow and enhance the mixing index. In general, active mixing technology can achieve higher mixing efficiency than passive mixing technology (Suh and Kang, 2010).

Loucaides *et al.* (2012) found that significant mixing and pumping effects of micromixer can be achieved by applying different AC voltages to the eight groups of electrodes set on the top and low walls alternatingly. Alipanah *et al.* (2017) studied the mixing efficiency of AC electroosmotic flow in a T-shaped micromixer. It was found that Newtonian fluids and non-Newtonian fluids at high flow rate could be mixed efficiently at shorter mixing lengths. Cao *et al.* (2008) analyzed the flow characteristics by applying alternating sine form current to the walls. The simulation results showed that the mixing efficiency depends on the AC potential applied on the walls and the arrangement of electrodes. The mixing efficiency can reach 98% at 10V with 16 pairs of electrodes. Luo *et al.* (2008) studied the flow behavior and mixing effect with different frequencies of AC signal on the two inlets of the T-type micromixer. It was found that the concentration was independent of the frequency, and there was no substantial increase in the mixing efficiency with microchannel width increasing. Keshavarzian *et al.* (2018) reported a new mixing chamber with a number of electrodes set on the inner and outer loops. It is found that the optimum mixing index can be achieved with electrodes placed on the loops in a cross-like pattern.

Samples' mixing in microchannels is difficult because of the low Reynolds number. So it may be necessary to apply high DC voltage on the microchannel to obtain high mixing efficiency, but high voltage could generate Joule heat and bubbles (Chao *et al.,* 2010b). The majority of active mixing strategies reported in the literatures are applying sinusoidal AC signal to the microchannels. Other types of AC signals have rarely been considered. It does not mean directly that sinusoidal AC field can make the best mixing. Other types of AC signals can also generate diverse distribution of electric field, which in turn affects the flow field and the mixing index. Thus, the present study analyzes and compares the flow features and mixing efficiency with different waveforms of AC/DC signals in microchannel by performing a series of simulations. Findings of this study can be utilized to developing electrokinetic mixers for

biological analysis such as drug screening where the efficiency of analyte mixing is vital.

2. PHYSICAL MODEL

The physical model is shown in Fig. 1. The inlet and outlet of the chamber is imposed with DC signals, and the upper and lower electrode plates receive DC or AC signals from the waveform generator. The microchannel is 1000 μm in length and 100 μm in width, and the electrode plate has a length of 100 μm, which is located in the middle of the upper or lower wall. Two different concentrations of fluids are pumped into the mixing chamber. The upper fluid is buffer solution, and the lower one is symmetric electrolyte potassium chloride (KCl) solution.
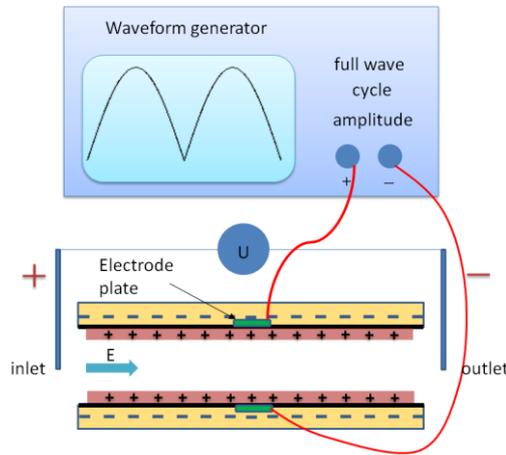

Fig. 1. Schematic diagram of devices.

2.1 Governing Equations

The fluid is assumed to be incompressible and viscous Newtonian fluid. The corresponding governing equations are as follows:

$$\nabla \cdot \mathbf{u} = 0 \tag{1}$$

$$\rho(\frac{\partial \mathbf{u}}{\partial t} + (\mathbf{u} \cdot \nabla)\mathbf{u}) = -\nabla p + \mu \nabla^2 \mathbf{u} + \rho_e \mathbf{E} \tag{2}$$

where $\mathbf{u}$ is the velocity, ρ is the density of the fluid, p is the pressure, μ is the dynamic viscosity, ρ_e is the net charge density, $\rho_e \mathbf{E}$ is the electric force acting on the fluid. The electric field strength $\mathbf{E}$ is related to the potential as follows:

$$\mathbf{E} = -\nabla(\varphi + \psi) \tag{3}$$

where ψ is the induced electrical potential of the EDL, and φ is the electrical potential applied at both ends of the micro channel.

The fluid is driven by the applied electric field, and its motion is governed by the Laplace equation:

$$\nabla^2 \varphi = 0 \tag{4}$$

In the electric double layer, the space charge distribution and the spatial potential can be calculated by the Poisson equation (Hunter, 1981):

$$\nabla^2 \psi = -\frac{\rho_e}{\varepsilon_r \varepsilon_0} \tag{5}$$

where ε_r is the relative dielectric constant of the electrolyte solution，and ε_0 is the vacuum dielectric constant.

The electric double layer potential and the concentration of ion i obey the Boltzmann distribution (Hunter, 1981):

$$n_i = n_{i\infty} \exp(-\frac{z_i e \psi}{k_B T_0})i \tag{6}$$

where e is the electron charge, z_i is the valence of ion i, k_B is the Boltzmann constant, T_0 is the absolute temperature, n_i is the ionic concentration of ion i, $n_{i\infty}$ is the density concentration of the ion i away from the wall (electrolyte solution). For the symmetric electrolyte solution, $|z_1|=|z_2|=z$, $n_{-\infty}= n_{+\infty}= n_\infty$. The charge density can be expressed as:

$$\rho_e = -2zen_\infty \sinh(-\frac{ze\psi}{k_B T_0}) \tag{7}$$

The ionic concentration is governed by the Nernst-Planck equation as follows：

$$\frac{\partial n_i}{\partial t} + \nabla \cdot J_i = 0 \tag{8}$$

$$J_i = \mathbf{u}_{n_i} - D_i \nabla n_i - \frac{z_i e D_i}{k_B T_0} n_i \nabla(\phi + \psi) \tag{9}$$

where J_i is the ionic flux of the ion species i, D_i is the diffusion coefficient of the ion i. The mixing of fluids is governed by the transport equation as follows (Ermakov *et al.,* 1998):

$$\frac{\partial C}{\partial t} + (\mathbf{u} + \mathbf{u}_{ep})\nabla C = D_c \nabla^2 C \tag{10}$$

$\mathbf{u}_{ep}$ is the electrophoresis speed of ion migration. C is the species concentration and D_c is the diffusion coefficient.

2.2 Boundary Conditions

The boundary conditions for the inlet are as follows:

$\varphi = \varphi_{in}$; $\mathbf{u} = 0$; $P = 0$; $C = 0$ (upper part of the entrance) or $C = 1 \, mol/L$ (lower part of the entrance)

$$(11)$$

φ_{in} is the DC potential applied to the inlet.

The boundary conditions at the outlet are:

$$\varphi = 0; \; P = 0; \; \frac{\partial C}{\partial \vec{n}} = 0; \; \frac{\partial \mathbf{u}}{\partial \vec{n}} = 0 \qquad (12)$$

At the wall, the no-slip condition is imposed and the corresponding boundary conditions are:

$$\mathbf{u} = 0; \; \vec{n} \cdot \nabla \phi = 0;$$
$$\vec{n} \cdot (-D\nabla C_i - \mathbf{u}_i C_i \nabla \varphi + \mathbf{u} C_i) = 0$$

$$(13)$$

The zeta potential of the electrode plate is negligible, for the upper electrode it is $V_i(t)$, and for the lower electrode it is $-V_i(t)$, where $V_i(t)$ is different periodic potential waveforms generated by the waveform generator. Four different waveforms of $V_i(t)$ are shown in Fig. 2.
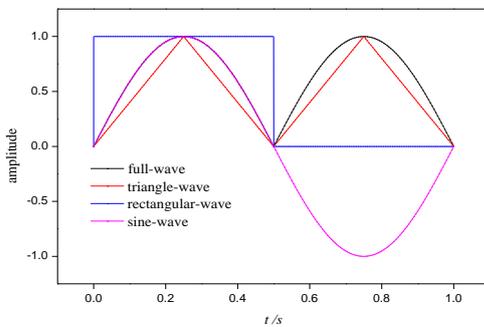

Fig. 2. Different potential waveforms.

2.3 Physical Parameters

To optimize the mixing efficiency in the microchannel, the frequency f is varied as 1 Hz, 2 Hz, 5 Hz, 10 Hz, 20 Hz and 50 Hz. Since high voltage imposed in the flow field will generate Joule heat to destroy the active cells, our research is focused on the low-voltage driven mixing, and the voltage V_0 is selected as 1 V, 3 V or 5 V. Other physical parameters are summarized in Table 1.

In order to evaluate the mixing effect of two different concentration solutions in

microchannel, the mixing efficiency (Huang *et al.,* 2014) is introduced as follows:

$$\sigma = \left(1 - \frac{\int_L \left| c - c_m \right| dy}{\int_L \left| c_0 - c_m \right| dy} \right) \times 100\% \qquad (14)$$

where σ is the mixing efficiency, it means complete mixing when it is 100% and no mixing when it is 0. c_m is the concentration of the complete mixing state, $c_m = 0.5 \, mol/m^3$. And c_0 denotes initial concentration at inlet, $c_0 = 0$ or $c_0 = 1 \, mol/m^3$ in this study, L refers to the height of the outlet.

Table 1 Physical parameters

(Symbol) Description	unit	Value
(ε_r) Relative permittivity	—	80
(ε_0) Permittivity of free space	$C^2 \cdot J^{-1} \cdot m^{-1}$	8.85×10^{-12}
(k_B) Boltzmann constant	$J \cdot K^{-1}$	1.38×10^{-23}
(e) Unit electron charge	C	1.60×10^{-19}
(T_0) Temperature	K	300
(n_∞) Everage concentration of ion	m^{-3}	6.02×10^{20}
(Z) Ionic valence	—	1
(ρ) Density	$kg \cdot m^{-3}$	1000
(μ) Dynamic viscosity	$Pa \cdot s$	9×10^{-4}
(ζ) Zeta potential	V	-0.075
(D_c) Diffusion coefficient	$m^2 \cdot s^{-1}$	1×10^{-11}
(φ_{in}) Inlet potential	V	3

2.4 Mesh and Validation

This simulation work was performed with finite element method (FEM) software: Comsol Multiphysics. The electrostatic potential, ion concentration, velocity, applied potential and pressure are discretized with linear elements. The electroosmotic flow in microchannels involves the multi-physics phenomena of fluid flow, electric field, and electrolyte ion transportation. The Navier–Stokes equation, Poisson equation,

and Nernst-Planck equation are coupled to solve in the numerical simulation of electroosmotic flows. The computational domain was meshed with 19362 triangle elements and grid refinement was employed at the boundary layer near the walls. Convergence test was performed with higher number of elements for steady-state solutions and the relative error was found to be negligible with the mesh employed.

In order to verify the accuracy of the simulation results, the electroosmotic flow in a two-dimensional channel caused by potential difference between inlet and outlet is simulated by solving Eqs. (1) - (7). Then the velocity of the mean flow is compared with the analytic solution of the Helmholtz-Smoluchowski equation (Park and Kim, 2009):

$$\mathbf{u} = -\frac{\varepsilon_0 \varepsilon_r \zeta}{\mu} \mathbf{E} \qquad (15)$$

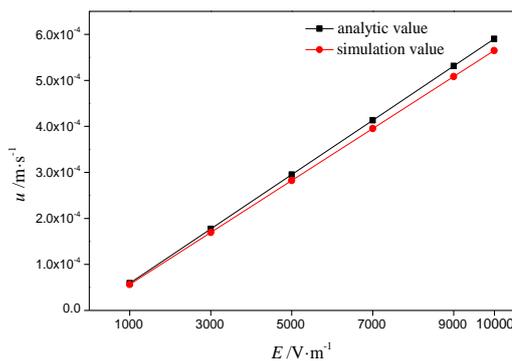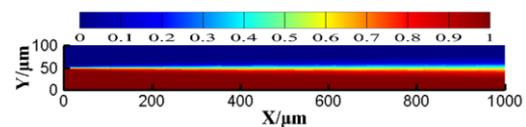As shown in Fig. 3, the simulation results agree well with the analytic solutions.

Fig. 3. Validation of the simulations.
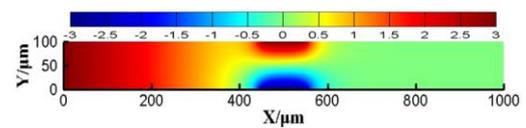
3. RESULTS AND DISCUSSIONS

3.1 Fluid Flow Condition under Applying DC on the Wall

In simulations, the DC voltage applied across the inlet and outlet of the microchannel is 3 V, and the corresponding electric field strength is about 3000 V/m. This value is lower than 20000 V/m in order to avoid the Joule heating effects (Mala and Li, 1999). As shown in Fig. 4(a), sample solution and buffer solution share a clear interface at the middle of the chamber, which presents a typical laminar flow with poor mixing efficiency. In order to improve the mixing efficiency, another DC elctric field is applied with 3 V voltage to the upper electrode and -3 V voltage to the lower electrode, electric potential is shown in Fig. 4(b). Due to the edge effect,
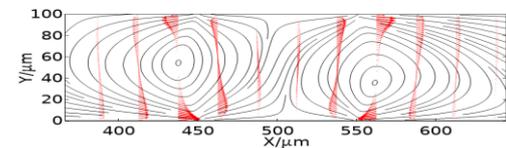
electric charges are mainly concentrated at the ends of electrode plates, where strong gradients of electric field are detected. A pair of vortices with oppisite rotating direction are formed near the electrode plates, as shown in Fig. 4(c). The steady laminar flow has been disturbed dramatically by these vortices and the mixing is greatly enhanced due to the increasing contact area and contact time between fluids, as shown in Fig. 4(d). After calculation, the mixing efficiency is found to be 81.23% at the outlet of the microchannel when external potential is applied to the walls.
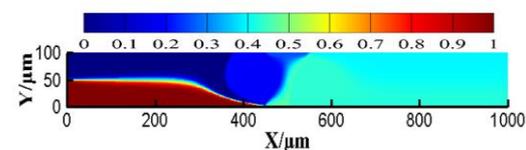

（a）concentration distribution in laminar flow

（b）Potential distribution

（c）streamline distribution

（d）concentration distribution in mixing

Fig. 4. Distribution of electric potential, streamline and concentrations of fluids under DC with 3000 V/m.

3.2 Analysis of Flow Field under Triangular-wave Potential

To improve further the mixing efficiency, an AC electric field is applied to the flow field combined with a DC electric field along the axis of the channel as the previous study. Different voltages and frequencies are considered in the simulations, as well as the waveforms of AC signals. A typical simulation result with V_0=3 V,
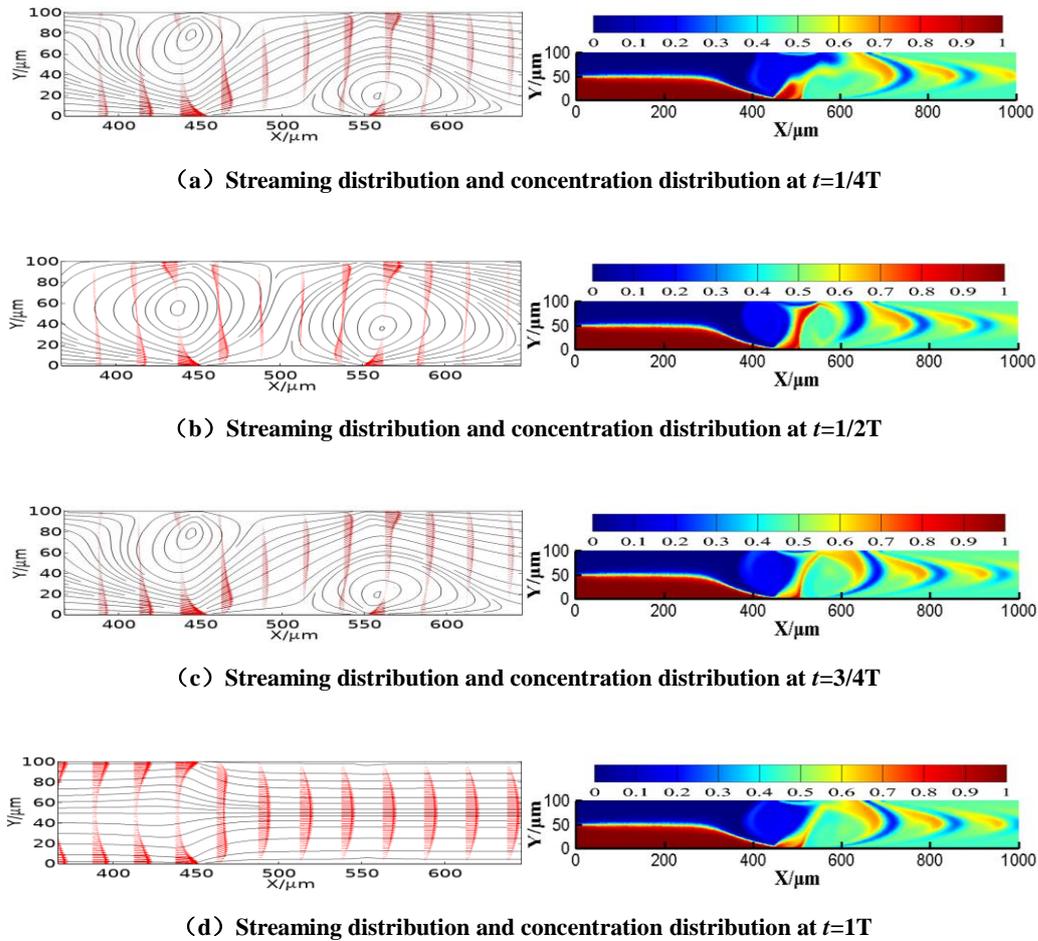
（a）Streaming distribution and concentration distribution at *t*=1/4T

（b）Streaming distribution and concentration distribution at *t*=1/2T

（c）Streaming distribution and concentration distribution at *t*=3/4T

（d）Streaming distribution and concentration distribution at *t*=1T

Fig. 5. Streaming distribution and concentration distribution in one triangular waveform at V_0=3 V and f=5 Hz.

f=5 Hz and triangular-waveform of AC signal is shown in Fig. 5, and micro-vortices are established by applying AC electric fields to the two electrodes. At different time, either a negative or a positive electrical potential gradient is formed in the region of the electrode-pair. In general, the flow direction should be from high potential to low potential. As shown in Fig. 5, this arrangement of voltages results in the formation of vortices different in size within the microchannel at different moment. The positions of the vortices are no longer fixed in space as the DC case, and the strengths of the vortices are changed with time. In the concentration distribution of Fig. 5, due to the interaction of one pair of vortices with opposite rotating directions, two different concentrations of fluids are mixed chaotically. High-concentration fluid and low-concentration fluid alternately appear in the middle zone of the microchannel and mix efficiently when flowing to the outlet. The recirculation flows shown in Fig. 5 are consistent with the results of Wu *et al.* (2007), which

further validate the accuracy of our simulations.

3.3 Analysis of Mixing Efficiency with Time at Different Frequencies

Figure 6 shows the variation of mixing efficiency with the evolution of time under different frequencies and waveforms. From Figs. 6(a)-(c), one can see that when the frequency f is relatively small, the mixing efficiency increases with time at first, and then it is nearly unchanged at the same phase of different cycles, this can be viewed as a stable periodic state of mixing. As shown in Figs. 6(d)-(f), the same situation is encountered at higher frequency, but the amplitudes of fluctuations in one cycle turn out to be small. The mixing efficiency can be achieved as high as 90% for full-wave signal. The sinusoidal potential has the lowest mixing efficiency, compared to the other three potential waveforms when $f \geq 10$ Hz. It can be seen that the time to reach the stable periodic state of mixing at $f \leq 10$ Hz is around 2 s, while it is around 1.6 s at $f = 20$ Hz and 1.3 s at $f = 50$ Hz.
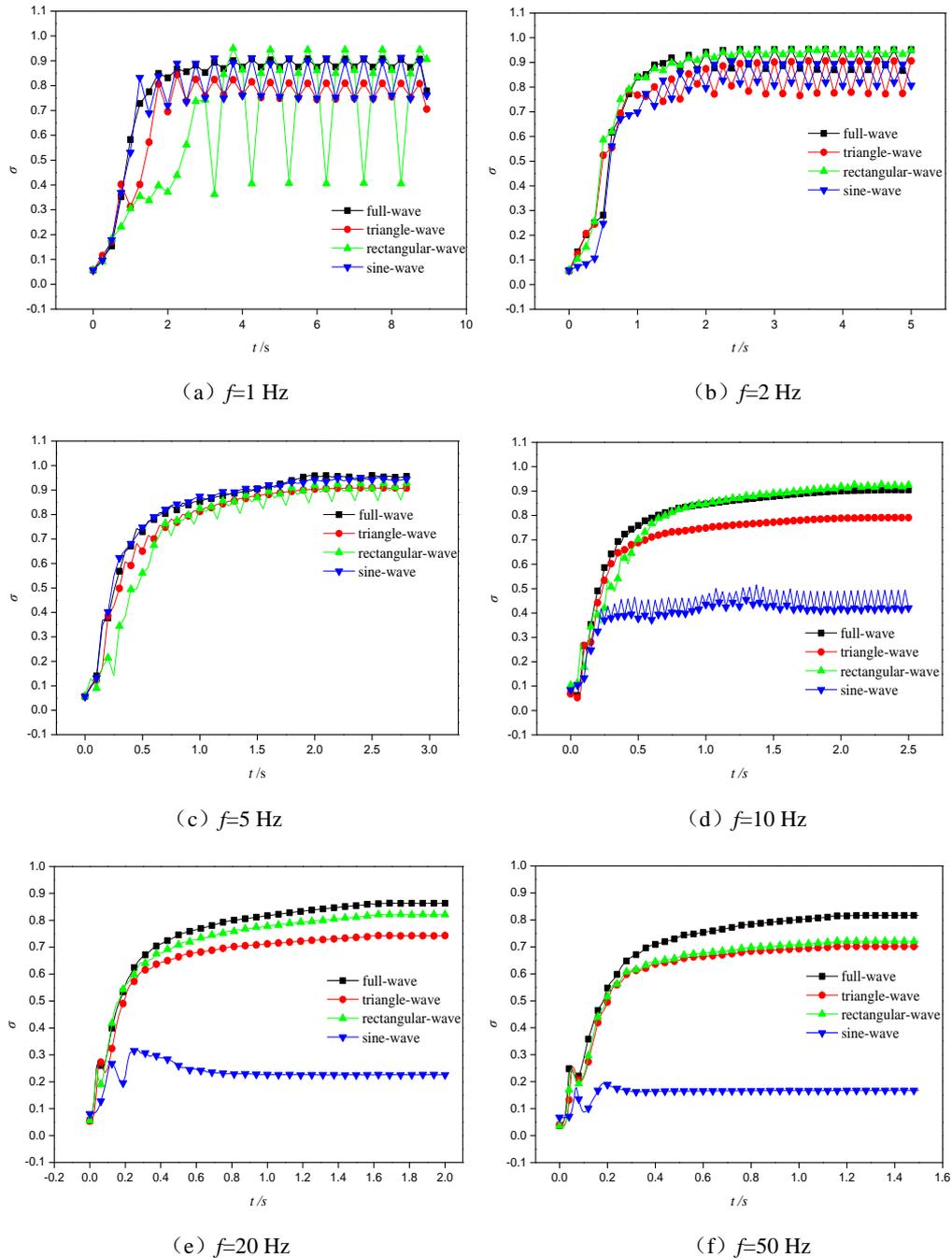
(a) f=1 Hz

(b) f=2 Hz

(c) f=5 Hz

(d) f=10 Hz

(e) f=20 Hz

(f) f=50 Hz

Fig. 6. Mixing efficiency of different waveform potentials.

3.4 Analysis of Mixing Efficiency with Frequency under Different Voltages

In order to study the effect of different waveforms on the mixing efficiency, an average mixing efficiency in one stable periodic mixing cycle is defined as follows:

$$\overline{\sigma} = \frac{1}{T} \int_{nT}^{(n+1)T} \sigma \, dt \qquad (16)$$

where T is one single period. The relationship of average mixing efficiency with frequency is shown in Fig. 7, and we find that the mixing efficiency increases significantly as the potential increases. The peak of mixing efficiencies at different voltages and frequencies are different. At $V_0 = 1$ V, the mixing efficiency reaches its maximum at $f = 2$ Hz, while at $V_0 = 3$ V, the mixing efficiency reaches its maximum about 90% at $f = 5$ Hz. When $V_0 = 5$ V, the maximum mixing efficiency is close to 95%, but the frequency to achieve that is not fixed in different waveforms. These findings are consistent with
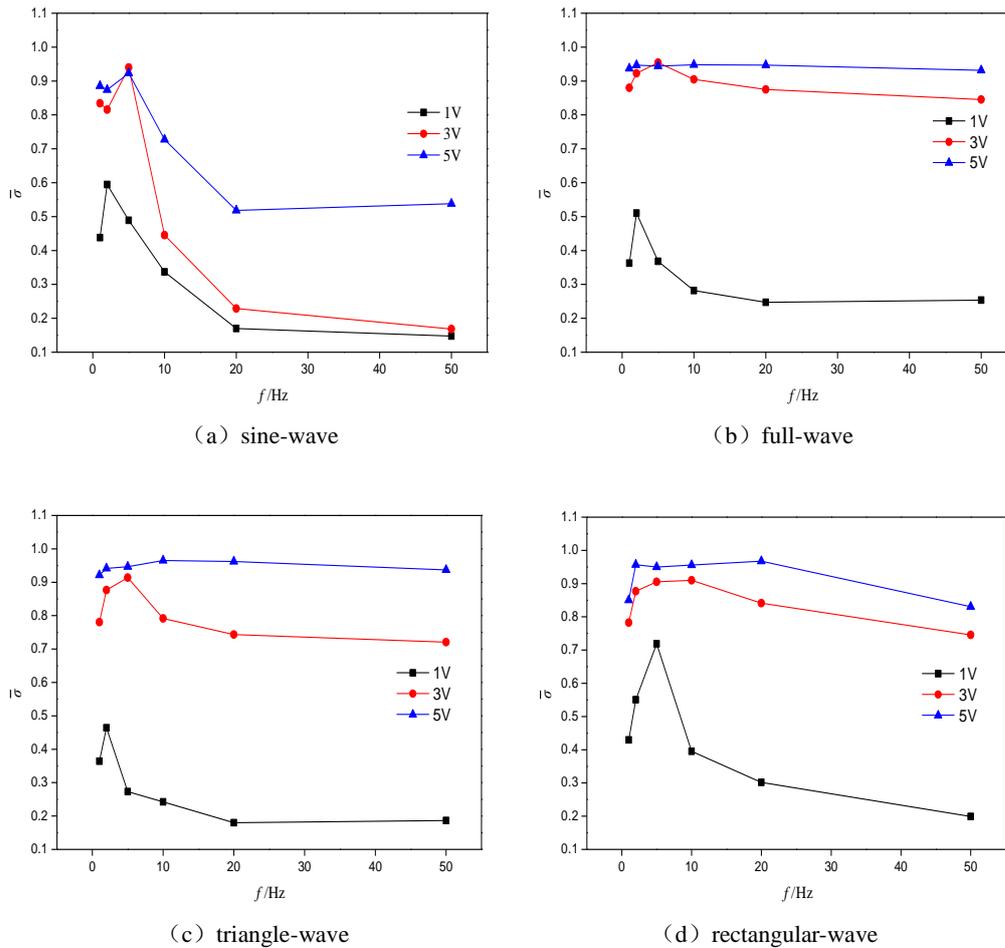
（a）sine-wave

（b）full-wave

（c）triangle-wave

（d）rectangular-wave

Fig. 7. Variation of mixing efficiency with frequency at different voltages.

the results of Fu *et al.* (2005). The mixing efficiency under sine-wave is the lowest one in every frequency except f =5 Hz, as shown in Fig. 7(a). Since the shape of triangular-wave is similar to that of full-wave, the mixing efficiency is more or less the same, as shown in Figs. 7(b)-(c). At V_0=3 V, where the mixing efficiency of the full-wave potential at each frequency is about 90%, it is generally higher than that of the other three potential waveforms. At V_0=5 V, where the mixing indexes of the full-wave, triangular-wave and rectangular-wave potentials are almost equal at middle of frequencies, it is about 95%, as shown in Figs. 7(b)-(d). In summary, the mixing under full-wave potential is the best, compared with the other three waveforms.

4. CONCLUSION

This paper has presented a novel micromixer for effective mixing via applying DC or different waveforms of AC signal on the electrode plates. The velocity and concentration distribution are analyzed, as well as the variation of mixing efficiency with time or frequency under different potential. The main conclusion is as follows:

(1) The vortices generated by the DC or AC field improve significantly the mixing efficiency of different concentrations fluids.

(2) The mixing efficiency rises with time and then reaches a stable periodic state for mixing efficiently. In one cycle of the stable state, the mixing efficiency fluctuates with time, and the amplitude of fluctuations is lower with increasing the frequency of voltages.

(3) A combination of 3 V AC full-wave potential with the frequency of 5 Hz on the electrode plates, are the most optimal parameters for mixing of incoming fluids with different concentrations.

REFERENCES

Alam, A., A. Afzal and K. Y. Kim (2014). Mixing performance of a planar micromixer with circular obstructions in a curved microchannel. *Chemical Engineering Research and Design* 92(3), 423-434.

Alipanah, M. and A. Ramiar (2017). High efficiency micromixing technique using periodic induced charge electroosmotic flow: A numerical study. *Colloids and Surfaces A: Physicochemical and Engineering Aspects* 524, 53-65.

Ansari, M. A., K. Y. Kim, K. Anwar and S. M. Kim (2012). Vortex micro T-mixer with non-aligned inputs. *Chemical Engineering Journal* 181, 846-850.

Auroux, P. A., D. Iossifidis, D. R. Reyes and A. Manz (2002). Micro total analysis systems. 2. Analytical standard operations and applications. *Analytical chemistry* 74(12), 2637-2652.

Cao, J., P. Cheng and F. J. Hong (2008). A numerical study of an electrothermal vortex enhanced micromixer. *Microfluidics and Nanofluidics* 5(1), 13-21.

Chao, K., B. Chen and J. K. Wu (2010a). Numerical analysis of field-modulated electroosmotic flows in microchannels with arbitrary numbers and configurations of discrete electrodes. *Biomedical microdevices* 12(6), 959-966.

Chao, K., J. K. Wu and B. Chen (2010b). Joule heating effect of electroosmosis in a finite-length microchannel made of different materials. *Applied Mathematics and Mechanics* 31(1), 109-118.

Chen, C. K. and C. C. Cho (2008). Electrokinetically driven flow mixing utilizing chaotic electric fields. *Microfluidics and nanofluidics* 5(6), 785-793.

Chen, X., T. Li and Z. Hu (2017). A novel research on serpentine microchannels of passive micromixers. *Microsystem Technologies* 23(7), 2649-2656.

Chen, X., T. Li, H. Zeng, Z. Hu and B. Fu (2016). Numerical and experimental investigation on micromixers with serpentine microchannels. *International Journal of Heat and Mass Transfer* 98, 131-140.

Cheng, Y., Y. Jiang and W. Wang (2018). Numerical simulation for electro-osmotic mixing under three types of periodic potentials in a T-shaped micro-mixer. *Chemical Engineering and Processing-Process Intensification* 127, 93-102.

Ermakov, S. V., S. C. Jacobson and J. M. Ramsey (1998). Computer simulations of electrokinetic transport in microfabricated channel structures. *Analytical Chemistry* 70(21), 4494-4504.

Fu, L. M., R. J. Yang, C. H. Lin and Y. S. Chien (2005). A novel microfluidic mixer utilizing electrokinetic driving forces under low switching frequency. *Electrophoresis* 26(9), 1814-1824.

Hamedi, A., M. Shamshiri, M. Charmiyan and E. Shirani (2016). Investigation of Nonlinear Electrokinetic and Rheological Behaviors of Typical Non-Newtonian Biofluids through Annular Microchannels. *Journal of Applied Fluid Mechanics* 9(1), 367-378.

Hossain, S., I. Lee, S. M. Kim and K. Y. Kim (2017). A micromixer with two-layer serpentine crossing channels having excellent mixing performance at low Reynolds numbers. *Chemical Engineering Journal* 327, 268-277.

Huang, K. R., Z. H. Hong and J. S. Chang (2014). Microfluidic mixing on application of traveling wave electroosmosis. *European Journal of Mechanics-B/Fluids* 48, 153-164.

Hunter, R. J. (1981). Zeta potential in colloid science: principals and applications. *Academic Press*, New York.

Kamali, R., S. A. Shekoohi and A. Binesh (2014). Effects of magnetic particles entrance arrangements on mixing efficiency of a magnetic bead micromixer. *Nano-Micro Letters* 6(1), 30-37.

Keshavarzian, B., M. Shamshiri, M. Charmiyan and A. Moaveni (2018). Optimization of an Active Electrokinetic Micromixer Based on the Number and Arrangement of Microelectrodes. *Journal of Applied Fluid Mechanics* 11(6), 1531-1541.

Lee, C. Y., C. L. Chang, Y. N. Wang and L. M. Fu (2011). Microfluidic mixing: a review.

International journal of molecular sciences 12(5), 3263-3287.

Lee, C. Y., W. T. Wang, C. C. Liu and L. M. Fu (2016). Passive mixers in microfluidic systems: A review. *Chemical Engineering Journal* 288, 146-160.

Lim, C. Y. and Y. C. Lam (2012). Analysis on micro-mixing enhancement through a constriction under time periodic electroosmotic flow. *Microfluidics and nanofluidics* 12(1-4), 127-141.

Loucaides, N., A. Ramos and G. E. Georghiou (2012). Configurable AC electroosmotic pumping and mixing. *Microelectronic Engineering* 90, 47-50.

Luo, W. J., K. C. Chang and J. S. Wang (2008). Proportional Mixing of Microfluidic Flows Utilizing DC and AC Electric Fields in a T-type Microchannel. *Journal of Applied Sciences* 8, 1632-1641.

Ma, Y., C. P. Sun, M. Fields, Y. Li, D. A. Haake, B. M. Churchill and C. M. Ho (2008). An unsteady microfluidic T-form mixer perturbed by hydrodynamic pressure. *Journal of Micromechanics and Microengineering* 18(4), 045015.

Mala, G. M. and D. Li (1999). Flow characteristics of water in microtubes. *International journal of heat and fluid flow* 20(2), 142-148.

Matías, A., O. Bautista, F. Méndez and P. Escandón (2018). Electroosmotic Pumping Between Two Immiscible Electrical Conducting Fluids Controlled by Interfacial Phenomena. *Journal of Applied Fluid Mechanics* 11(3), 667-678.

Nekoubin, N. (2018). Electroosmotic flow of power-law fluids in curved rectangular microchannel with high zeta potentials. *Journal of Non-Newtonian Fluid Mechanics* 260, 54-68.

Park, H. M. and T. W. Kim (2009). Extension of

the Helmholtz-Smoluchowski velocity to the hydrophobic microchannels with velocity slip. *Lab on a Chip* 9(2), 291-296.

Rashidi, S., H. Bafekr, M. S. Valipour and J. A. Esfahani (2018). A review on the application, simulation, and experiment of the electrokinetic mixers. *Chemical Engineering and Processing-Process Intensification* 126, 108-122.

Shamloo, A., P. Vatankhah and A. Akbari (2017). Analyzing mixing quality in a curved centrifugal micromixer through numerical simulation. *Chemical Engineering and Processing: Process Intensification* 116, 9-16.

Stone, H. A., A. D. Stroock and A. Ajdari (2004). Engineering flows in small devices: microfluidics toward a lab-on-a-chip. *Annual Review of Fluid Mechanics* 36, 381-411.

Suh, Y. K. and S. Kang (2010). A review on mixing in microfluidics. *Micromachines* 1(3), 82-111.

Wang, Y., J. Zhe, P. Dutta and B. T. Chung (2007). A microfluidic mixer utilizing electrokinetic relay switching and asymmetric flow geometries. *Journal of Fluids Engineering* 129(4), 395-403.

Wu, C. H., J. K. Chen and R. J. Yang (2007). Electrokinetically driven flow control using bare electrodes. *Microfluidics and Nanofluidics* 3(4), 485-494.

Xie, Z. Y. and Y. J. Jian (2017). Entropy generation of two-layer magnetohydrodynamic electroosmotic flow through microparallel channels. *Energy* 139, 1080-1093.

Yaralioglu, G. G., I. O. Wygant, T. C. Marentis and B. T. Khuri-Yakub (2004). Ultrasonic mixing in microfluidic channels using integrated transducers. *Analytical chemistry* 76(13), 3694-3698.